Palaeogeography, Palaeoclimatology, Palaeoecology 514 (2019) 18–30

Contents lists available at ScienceDirect

Palaeogeography, Palaeoclimatology, Palaeoecology

journal homepage: www.elsevier.com/locate/palaeo

Are there ancient soils in the 3.7 Ga Isua Greenstone Belt, Greenland?

Gregory J. Retallack[a,*], Nora Noffke[b]

[a] Department of Geological Sciences, University of Oregon, Eugene, OR 97403-1272, USA
[b] Ocean, Earth & Atmospheric Sciences, Old Dominion University, Norfolk, VA 23529, USA

ARTICLE INFO

Keywords:
Paleosol
Archean
Paleoclimate
Atmospheric chemistry
Ancient life

ABSTRACT

A lens of black schist within 3.7 Ga quartzites of Greenland may be Earth's oldest known alluvial paleosol. The suspect metamorphic rock is a lens in orthoquartzite of berthierine schist with crystals of ripidolite, but it has a truncated top above dark gray grading down to gray color, ptygmatically folded surface cracks filled with silt grains, and large sand crystals, unusual for sedimentary or metamorphic rocks. The paleosol hypothesis was tested with thin sections showing plausible mineral weathering trends, and by chemical analysis showing molar weathering ratios and REE distribution like those of soils. The schist is deeply weathered and at the culmination of weathering trends from analysis of other metasediments of the Isukasia area. The protolith can be reconstructed as a saponite clay with a salt-rich horizon of kieserite, like other acid-sulfate paleosols of the early Earth. Models for proton and electron consumption of paleosols applied to the profile reveal an atmosphere with only 36 ± 510 ppm O_2 and 820 ± 201 ppm CO_2, and humid, cool temperate paleoclimate. The profile has organic $\delta^{13}C_{PDB}$ consistently of −24.2 to −27.4‰, and modest Raleigh distillation near the top. Similar consistent values and trends are produced by decay of organic matter in living soils, but biotic carbon isotopic composition of sediments is erratic from bed to bed, and abiotic carbon compounds of meteorites differ dramatically for each kerogen particle. Thus life in this very ancient soil is not precluded by our analyses, but ultrastructural and geochemical testing of carbon particles would further test this hypothesis.

1. Introduction

Soil formation is a combination of physical, chemical, or biological processes important for regulating planetary atmospheres, and the ultimate source of essential nutrients such as phosphorus for the nutrition and origin of life (Retallack, 2016a). Precambrian paleosols are evidence for the early history of our planet, including the composition of the atmosphere (Sheldon, 2006) and the antiquity of life on land (Djokic et al., 2017; Retallack, 2018). This study documents a lens of schist in quartzite from southwestern Greenland, and tests the hypothesis that this is the oldest known alluvial paleosol. Also explored are implications of this hypothesis for its chemical, biotic and sedimentary environment.

Hundreds of Precambrian paleosols are now known from major geological unconformities (Rye and Holland, 1998), but unconformity paleosols, even of Cenozoic age, can be confusing because of long duration of formation encompassing changes in formative conditions (Retallack, 2010). By any model of soil formation, the thick Precambrian profiles would have been thin at the beginning of their formation (Retallack et al., 2000), but only recently have thin alluvial Precambrian paleosols been widely recognized (Nabhan et al., 2016; Retallack et al., 2016; Retallack, 2018). Precambrian paleosols within sedimentary sequences have advantages as guides to past conditions because their formation times are of the order of millennia and their sedimentological context contributes to their interpretation. Short formation times are important for calculating atmospheric oxygen and carbon dioxide levels (Sheldon, 2006). Sedimentary settings are important for assessing ancient drainage conditions and sedimentation rates (Retallack et al., 2000). Recognizing paleosols in rocks as old and metamorphically altered as many Precambrian sequences can be challenging because they lack diagnostic features such as root traces (Retallack, 2016b). This paper outlines a variety of petrographic and geochemical techniques for recognition of soil profiles in metamorphic rocks.

Precambrian paleosols in alluvial facies have been hiding in plain sight for many years as deposits of “intermittently exposed environments” (Buick and Dunlop, 1990) and “salinas” (Lowe and Worrell, 1999). From a soil science perspective, however, salinas and playa lakes are dry more often than wet, and classified in soil maps as Solonchaks (Food and Agriculture Organization, 1974) or Gypsids (Soil Survey Staff, 2014). Although some sediment is delivered during short episodes of playa lake filling, most sediment is delivered to playas by wind, and

* Corresponding author.
E-mail address: gregr@uoregon.edu (G.J. Retallack).

https://doi.org/10.1016/j.palaeo.2018.10.005
Received 6 July 2018; Received in revised form 4 October 2018; Accepted 5 October 2018
Available online 09 October 2018
0031-0182/

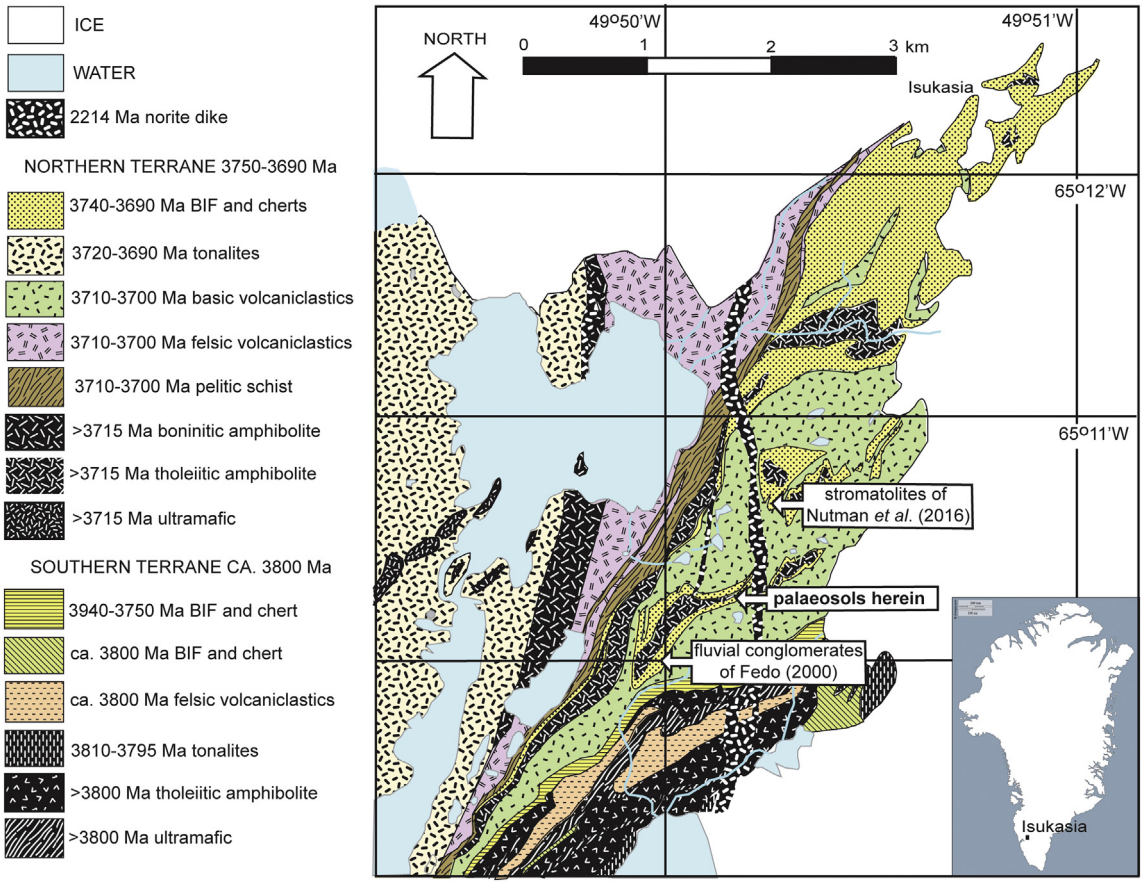

Fig. 1. Location of 3.7 Ga paleosols within the conglomerate-sandstone sequence of the Isukasia area, Greenland. (Modified from Arai et al. (2015).)

the subaerial weathering of that material and growth of salts are essentially soil-forming processes (Benison and Bowen, 2013, 2015). An additional semantic barrier to recognition of Precambrian alluvial soils is common definition of soils as a medium for life, which is difficult to assess in soil-like materials before the evolution of plants and on other planets (Certini and Ugolini, 2013). This study takes a broader view of soil as material altered by physical, chemical or biological processes on a planetary surface (Rye and Holland, 1998; Retallack, 2016a). Our effort to investigate the possibility of life in a Precambrian paleosol using carbon isotopic profiling is inconclusive, but permissive, and a first step in investigating an important question that should not be confused with an assumption.

2. Geological setting

The putative paleosol was discovered in a strike ridge of quartzite at N65.173485° W49.812884°, 1 km north of a red shelter hut by a small lake at N65.170331° W49.814642°, and south of a strike ridge of amphibolite, in the northeast limb of the Isua Greenstone Belt of southwestern Greenland, near the Isukasia iron ore mine (Fig. 1). This area exposes large volumes of oceanic pillow basalt, but also a thin supracrustal sequence of sedimentary rocks (Nutman and Friend, 2009; Nutman et al., 2015; Arai et al., 2015).

A lens of dark gray schist in quartzites (Fig. 2A) was identified as a possible paleosol in low ridges at N65.173485° W49.812884°, within a kilometer of outcrops of fluvial conglomerate (Fedo, 2000; Nutman et al., 2012) at N65.170002° W49.816485° and stromatolites (Nutman et al., 2016) at N65.179167° W49.804167°. Also nearby are banded iron formations, now widely interpreted as aquatic deposits formed by photoferrolysis within the photic zone (Konhauser et al., 2002; Crowe et al., 2008; Pufahl et al., 2013). This tract of quartzose sandstones and conglomerates was not ancient ocean floor or deep marine deposits, but has been interpreted as a coastal plain and shallow marine shelf (Fedo, 2000; Nutman et al., 2012, 2016). The putative paleosol is in a sequence of dolostones, quartzites and banded iron formation containing zircons with U-Pb ages of 3.699 ± 0.012 and 3.691 ± 0.006 Ga, unconformably above 3.709 ± 0.009 Ga andesitic metavolcanic rocks (Nutman et al., 2015). These rocks were altered by amphibolite facies metamorphism to 390 °C at ca.3.69 Ga (Rollinson, 2002: Nutman et al., 2012; Arai et al., 2015).

3. Materials and methods

The putative paleosol is a lens of dark gray schist within white quartzites, collected in the field as a single slab. Oriented thin sections and other rocks are archived as specimens in the Condon Collection of the Museum of Natural and Cultural History of the University of Oregon, in Eugene, Oregon. Thin sections of the schist and of overlying sandstone (Figs. 3–4) were point counted (500 points) using a Swift automated stage and Hacker electronic counting box to determine grain size categories (Supplementary information Table S1) and mineral composition (Table S2). Error on such 500 counts is ± 2% for common components (Murphy, 1983). Soil microfabric descriptive terminology in Table S1 is from Brewer (1974). Texture in Table S1 is from Soil Survey Staff (2014). Major and trace element chemical analyses were performed by ICP-AES on glass discs, using Bancroft granodiorite as a standard, and FeO by Pratt titration from ALS Geochemistry of Vancouver, British Columbia (Tables S3-S5). Bulk densities were determined from 20 to 40 g samples using paraffin by Retallack at the University of Oregon (Table S3). Errors (1 standard deviation) are from

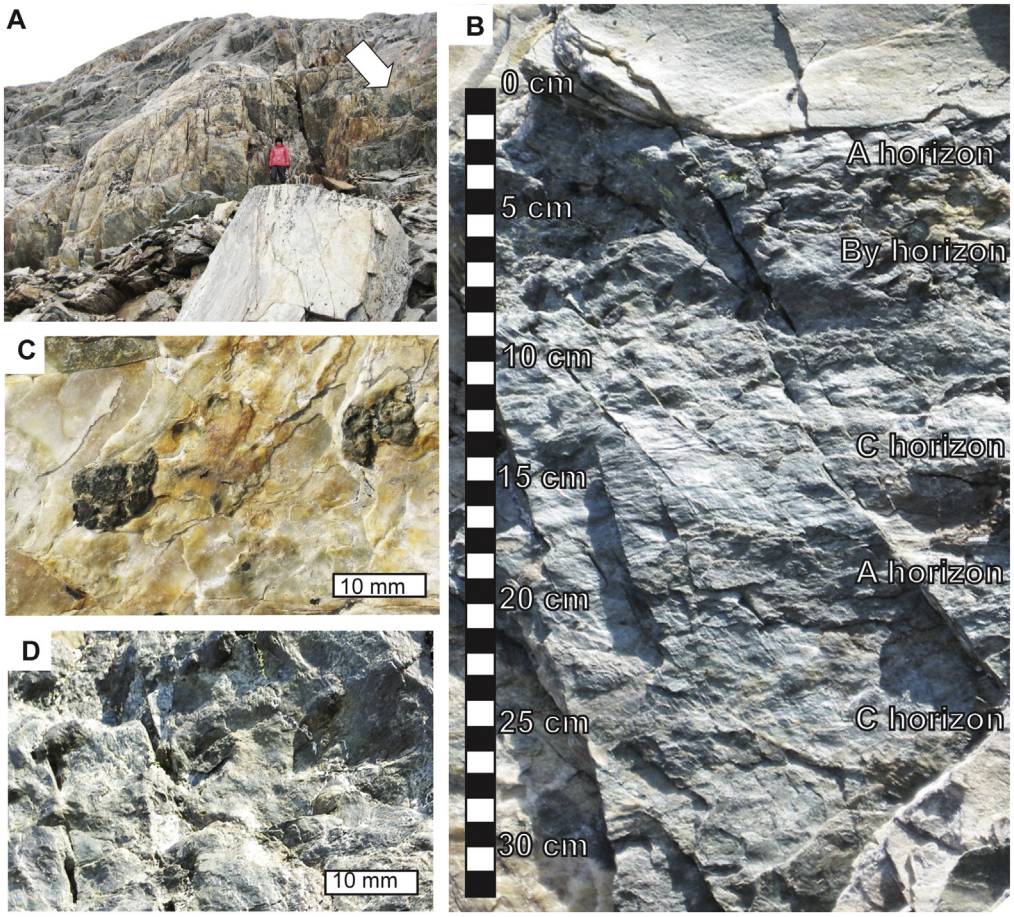

Fig. 2. Field and petrographic appearance of 3.7 Ga paleosols from Isukasia, Greenland: B, paleosol lens at arrow within quartzites; B, field view of Isi paleosol (A-By-C) profile above Pukit (A–C) profile; C, biotite schist clasts within quartzites and paleosol locality; D, field photograph of crystal pseudomorphs;

duplicate analyses, and 10 separate measurements of the same sample (R5316) for bulk density.

Polished thin sections were analyzed and mapped using a CAMECA SX100 microprobe. Their chemical composition was determined using the Cameca SX100 electron microprobe by J.J. Donovan in the Center for Advanced Materials Characterization of Oregon (CAMCOR) at the University of Oregon. An area 2.5 by 6 mm on a polished thin section was geochemically mapped spanning a part of a poikiloblastic crystal and its phyllosilicate matrix. Two separate runs were made on a grid 506 by 1200 pixels using 5 tunable wavelength dispersible spectrometers at 15 keV and 30 nA for a total of 10 elements. The beam was 1 μm diameter and dwell time of 30 s per pixel. Mean atomic number background intensity was calibrated and corrected for continuum absorption for each element analyzed (Donovan and Tingle, 1996;

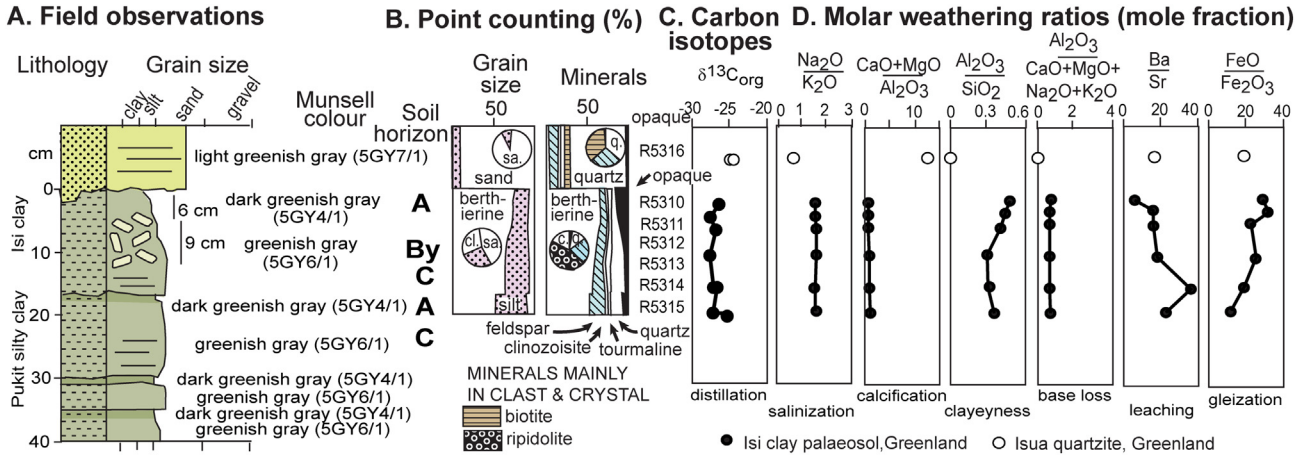

Fig. 3. Geochemical and petrographic data on a 3.7 Ga paleosol from Isukasia, Greenland: A, Field sketch and Munsell color; B, grain size and mineral composition was determined by counting 500 points in petrographic thin sections of matrix, and (in circles) clasts and sand crystals; C, carbon isotopic composition (‰) is relative to Vienna Peedee Belemnite; D, molar weathering ratios are from XRF analyses of whole rock. (For interpretation of the references to color in this figure legend, the reader is referred to the web version of this article.)

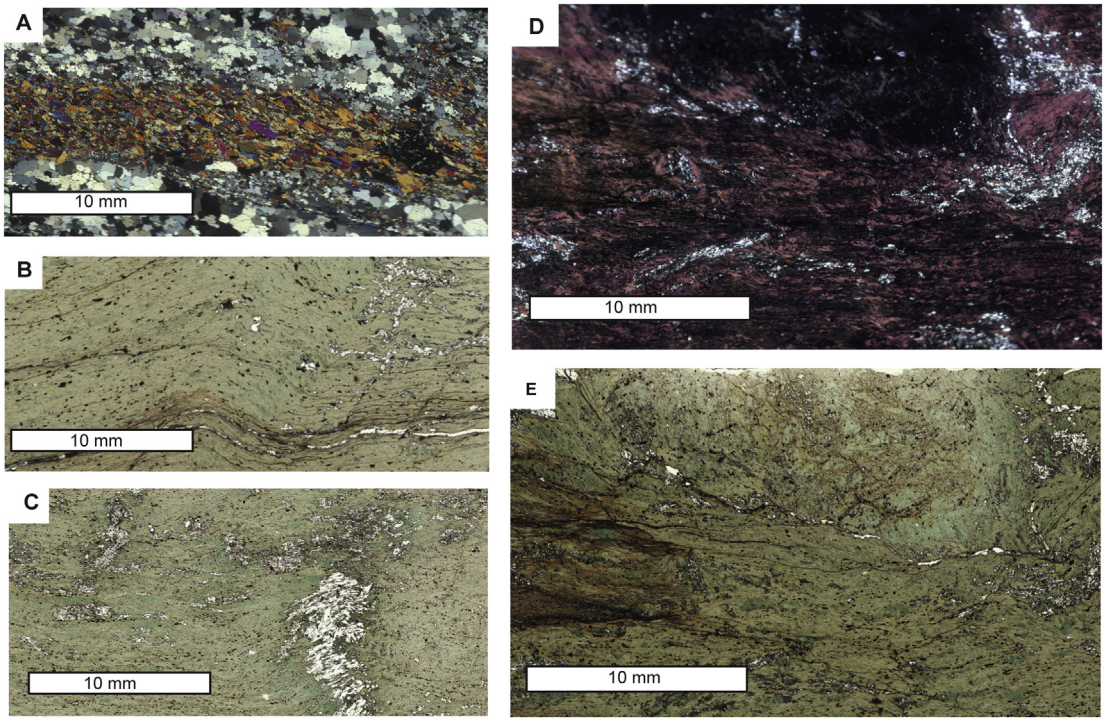

Fig. 4. A–E, petrographic thin section scans; A, clast of biotite schist in overlying quartzites (X-nicols); B, quartz-silt-filled tapering cracks (not quartz veins with interlocking, wall-concordant crystals) in surface horizon (plane light); C, quartz-silt-filled cracks (not quartz veins) in lower surface horizon (plane light); D, crystal pseudomorph (upper center X nicols); E, crystal pseudomorph (upper center plane light). Specimens in Condon Collection of Museum of Natural and Cultural History of the University of Oregon are R5316 (A), R5310 (B), R5315 (C), and R5312 (D–E).

Donovan et al., 2016). Interference corrections were applied to Mg for Ca interference, and to Ba for Ti interference (Donovan et al., 1993). Results are the average of 2 points and detection limits in weight percent were 0.006 for Ca kα, 0.007 for K kα, 0.01 for MgO, 0.025 for Fe kα and 0.04 for Ti kα. Analytical sensitivity (99% level) is 0.14% for Ba kα, 0.741% for Si kα, 2.295% for K kα, 7.232% for Ti kα, and 76.857% for Fe kα. Oxygen equivalent for halogens (F, Cl, Br, I) was not subtracted in matrix correlation. The matrix correction method was ZAF or Phi-Rho-Z calculations (Armstrong, 1988). Clustering of analyses into six distinct mineral phases was done by a modified k-means clustering method of J.J. Donovan.

Carbon stable isotopic composition of schist samples was measured by M. Yun of the University of Manitoba. Total organic carbon was low in the samples as determined by Eltra Helios EA in Manitoba, and also by LECO at ALS Geochemistry of North Vancouver, British Columbia. Assays for sulfur and nitrogen also were attempted, but amounts were insufficient for isotopic measurements. Calibration for organic carbon isotopic composition (Table 1) using a Varian Liberty 200 ICP-OES was performed by analyzing two international standards (USGS40, USGS41) at the beginning, middle and end of each run. A calibration line was calculated by least squares linear regression using the known and measured isotope values of the calibration standards. To monitor the quality of sample preparation (decarbonation by 6 N HCl) and analysis performance, an international standard USGS Green River shale SGR-1b ($\delta^{13}C_{org} = -29.3 \pm 0.1‰$ VPDB) was treated and analyzed with unknown samples. Replicate analyses of SGR-1b standard yielded the results of $\delta^{13}C_{org} = -29.6 \pm 0.1‰$ (n = 4).

4. Paleosol tests for the schist bed

The schist was suspected as a paleosol in the field because of its sharp erosional top above diffuse changes in texture (soil horizons: Fig. 2B), silt-filled fissures like mudcracks (Fig. 4B, C), and structures reminiscent of sand crystals (soil structure: Figs. 2D, 5). Microprobe mapping (Figs. 6–7, Table 2) revealed that the crystals are now an iron-magnesium aluminosilicate identical to the metamorphic mineral

Table 1
Sulfur, carbon, and stable isotopic composition of paleosols from Greenland.

Paleosol	Horizon	Sample	S_{total} (%)	C_{total} (%)	$C_{inorganic}$ (%)	$C_{organic}$ (%)	$\delta^{13}C_{organic}$ (‰ vs VPDB)
Isi	A	R5310	< 0.01	0.083	0.05	0.083	−26.20
Isi	A	R5311	< 0.01	0.009	0.02	0.009	−27.37
Isi	By	R5312	< 0.01	0.024	< 0.02	0.024	−26.60
Isi	By	R5313	0.01	0.031	< 0.02	0.031	−27.42
Pukit	A	R5314	< 0.01	0.028	< 0.02	0.028	−26.92
Pukit	A	R5314	< 0.01	0.028	< 0.02	0.028	−26.45
Pukit	C	R5315	< 0.01	0.035	< 0.02	0.035	−26.99
Pukit	C	R5315	< 0.01	0.021	< 0.02	0.021	−25.01
Cover		R5316	< 0.01	0.094	< 0.02	0.094	−24.71
Cover		R5316		0.094	0	0.094	−24.22

Note: $\delta^{13}C$ analysis after acid digestion was from continuous flow isotope ratio mass spectrometry (CF-EA-IRMS) by Misuk Yun of the University of Manitoba. Total carbon is by acid digestion followed by LECO furnace loss on ignition, and total S by nitric and hydrochloric acid leach and gravimetric finish from ALS minerals of Vancouver, British Columbia.

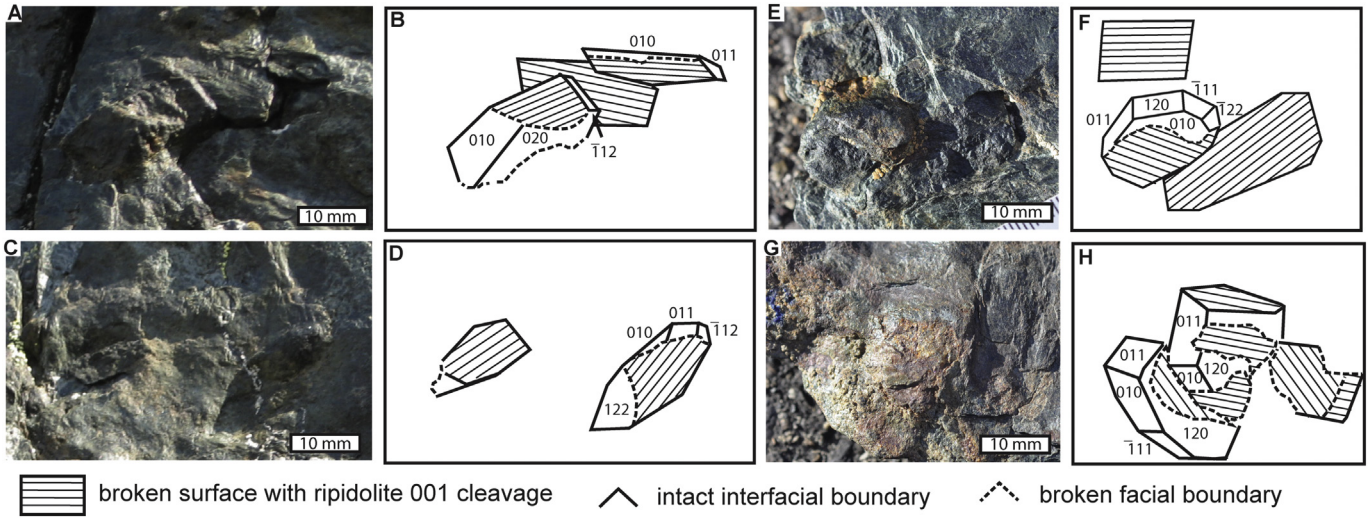

Fig. 5. Monoclinic crystal form of poikiloblasts in Isi clay paleosol.

ripidolite (ferroan clinochlore [$(Mg,Fe,Al)_6(Si,Al)_4O_{10}(OH)_8$]), and their matrix is the ferrous phyllosilicate berthierine (septechamosite [$(Fe^{2+},Fe^{3+},Al)_3(Si,Al)_2O_5(OH)_4$]). Poikiloblastic ripidolite has been recognized in these rocks as a metamorphic mineral, not an original phase (Rollinson, 2002). It may be a pseudomorph of a soluble mineral comparable with sand crystals of evaporites, now widely documented in other Archaean paleosols (Nabhan et al., 2016; Retallack et al., 2016; Retallack, 2016b, 2018).

Point counting of thin sections demonstrated that the most clayey portion of the profile was near the top, and was inversely proportional to feldspar decline (Fig. 3B), as would be expected from chemical weathering (Retallack, 2018). Thin sections also reveal ptygmatically folded clastic dikes of silt-size quartz, similar to soil cracks filled with loess, and then folded by burial compaction (Fig. 4B, C). Molar weathering ratios show gradual changes, rather than abrupt sedimentary discontinuities (Fig. 3D), and this also is a feature of paleosols

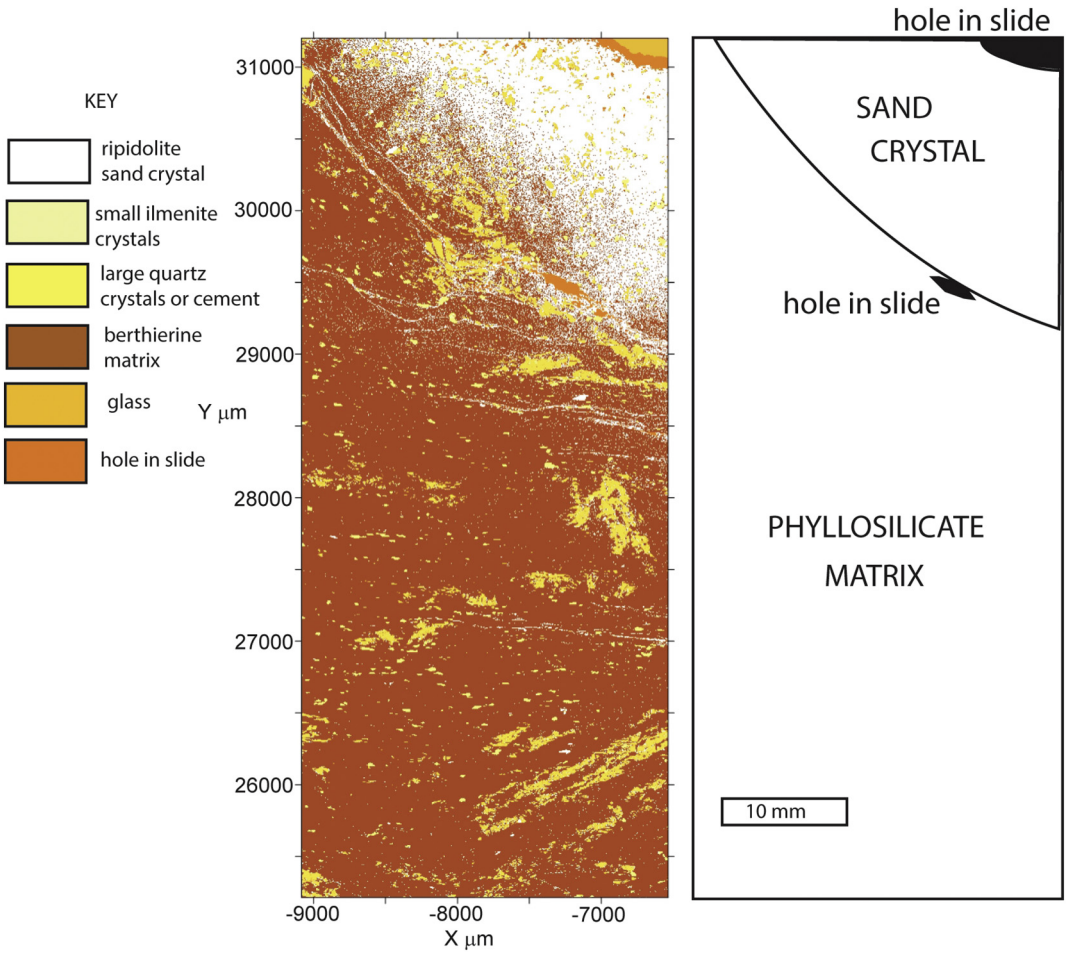

Fig. 6. Microprobe map of mineral phases in crystal pseudomorph and matrix of Isi clay paleosol.

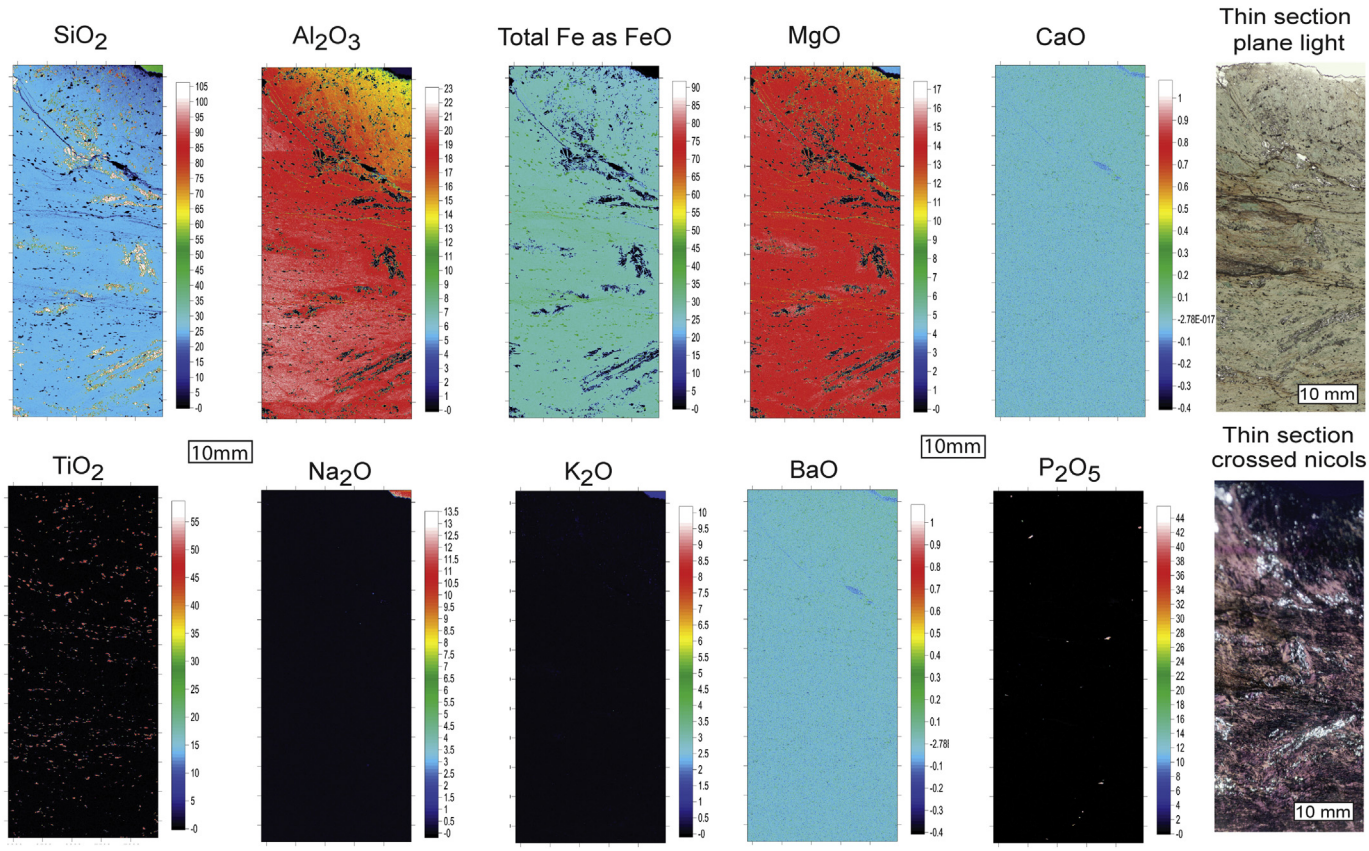

Fig. 7. Microprobe maps of major oxides in crystal pseudomorph and matrix of Isi clay paleosol.

rather than sedimentary bedding (Retallack, 2016b). The isotopic composition of organic carbon ($\delta^{13}C_{org}$ in Fig. 3C) also shows little variation within the profile as in soils (Wynn, 2007).

Rare earth element analyses show light rare earth depletion near the surface, but enrichment in the subsurface (By) horizon (Fig. 8), as expected in soils (Retallack, 2016b). Furthermore, these rocks lack the large positive europium anomaly of hydrothermally altered rocks (Sugahara et al., 2010), although positive europium anomalies are found in other Isua Greenstone Belt rocks (Appel, 1983; Bolhar et al., 2005). Our schist profile is at the end of a trend of weathering found in other metasediments and metabasalts of the Isukasia area of Greenland (Fig. 9).

A diagnostic tool for identifying soils and paleosols and differentiating them from sediments and hydrothermally altered rocks is tau analysis (Brimhall et al., 1992), in which overall mass gains and losses (strain or epsilon) are plotted against specific elemental mass gains and losses (mass transfer or tau). Equations for calculating strain (epsilon) and mass transfer (tau) are shown in Table 3. Tau analysis shows negative strain and depletion of most elements (Fig. 10), like other paleosols and soils (Retallack et al., 2016; Retallack, 2018).

Thus all eight petrographic and geochemical tests of the paleosol hypothesis for this bed fail to support the null hypothesis that it was just

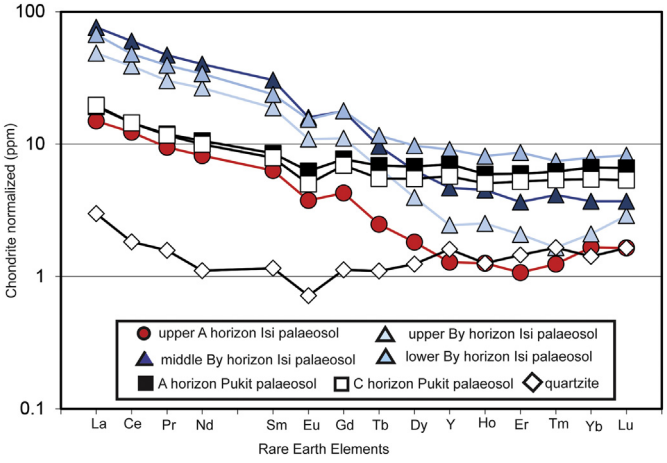

Fig. 8. REE analyses of 3.7 Ga paleosols from Isukasia, Greenland. Moderately developed Isi paleosol shows greater surface REE depletion than very weakly developed Pukit paleosol, and both lack positive europium anomaly of hydrothermal alteration.

Table 2
Analyses of mineral phases in 3.7 Ga Isi paleosol by ion microprobe.

	SiO_2	TiO_2	Al_2O_3	Fe total as FeO	CaO	MgO	Na_2O	K_2O	P_2O_5	BaO
Berthierine	24.47	0.13	38.06	28.05	0.00	21.19	0.02	0.00	0.01	0.01
Holes	5.50	0.08	5.14	4.84	0.14	3.05	0.34	0.03	0.04	0.06
Epoxy resin	59.06	0.13	15.19	12.86	0.43	9.75	1.90	0.14	0.00	0.00
Quartz crystals and cement	96.14	0.03	1.89	1.71	0.01	0.93	0.02	0.00	0.00	0.00
Ilmenite crystals	2.78	35.39	3.74	43.26	0.01	2.54	0.02	0.00	0.00	0.03
Ripidolite sand crystal	23.36	0.09	31.06	25.40	0.24	19.60	0.02	0.03	0.35	0.00

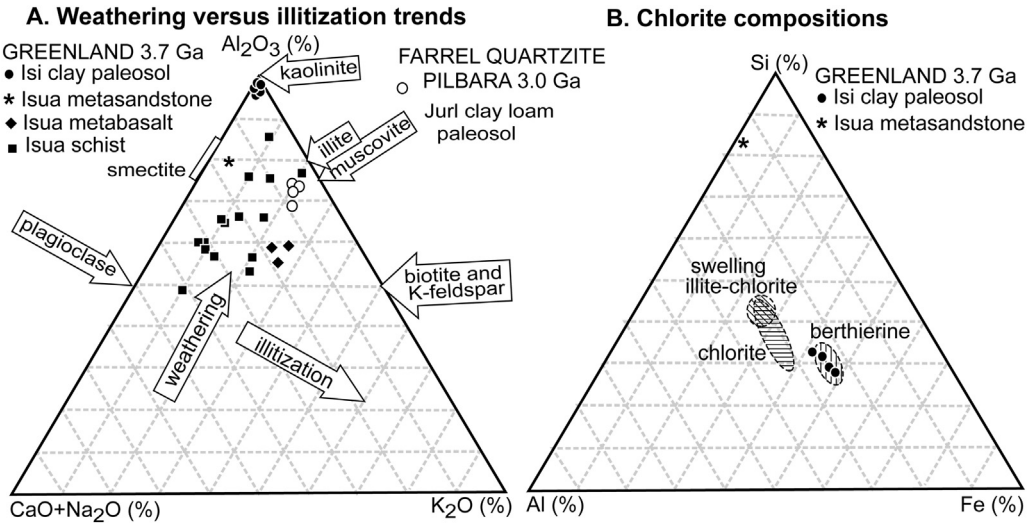

Fig. 9. Weathering trends and chlorite compositions in paleosols and sedimentary rocks from the Isua Greenstone Belt: A, comparison of Isi paleosol with other paleosols (Retallack et al., 2016; Retallack, 2018), and weathering trends in associated metasediments (Arai et al., 2015); B, Isi paleosol and sandstone compositions compared with other chlorites (Jahren and Aagaard, 1989).

a shale bed: (1) field appearance, (2) crack fills and other structures, (3) textural profile, (4) mineral profile, (5) molar ratios, (6) carbon isotopic composition, (7) REE trends, and (8) tau analysis.

5. What else could it be?

Although the schist bed passes eight tests as a paleosol, other possibilities deserve consideration. In high grade metamorphic terrains like the Isua Greenstone Belt, alternatives could include structural boudin, fault mylonite, or hydrothermal aureole. Boudins are remnants of beds that have been stretched and attenuated into lozenges by extreme extensional deformation (Goscombe and Passchier, 2003; Schenk et al., 2007). The Greenland bed studied is a schist within a quartzite, but most boudins are harder rock remnants in softer matrix. Nor does the analyzed bed have sheathing folds, displaced margins, or marginal shearing of boudins.

Mylonites are intervals of crushed rock and breccia created by the grinding action of large faults planes (Reed, 1964; Evans and White, 1984). Our thin sections and specimens revealed no breccia, but rather large poikiloblastic crystals (Figs. 5–6). Mylonites chemically homogenize rocks, but our chemical analyses reveal changes compatible with weathering (Figs. 8–10) and berthierine clay rather than rock flour (Figs. 6–7).

Hydrothermal aureoles are pockets of intense, high-temperature, fluid alteration near ore bodies or quartz veins (Loucks et al., 1988; Hannington et al., 2003). Neither quartz veins, nor sulfide ores were seen and the alteration was asymmetric down from a truncated surface rather than symmetrical around high temperature minerals (Fig. 3). Hydrothermal alteration is also ruled out by lack of europium anomaly (Fig. 8: Sugahara et al., 2010) and carbon isotopic values within the range of unaltered organic matter (Fig. 3: Rosing, 1999; Grassineau et al., 2006).

6. Peering through severe metamorphic alteration

Severe metamorphic alteration of the schist is apparent from pervasive schistosity obvious in the field (Fig. 2) and thin section (Fig. 4), but burial diagenetic change must also be considered before reconstructing the original profile. Burial illitization can alter paleosol chemical composition, and should divert chemical trends away from alumina enrichment toward potash enrichment (Novoselov and de Souza Filho, 2015). This was not observed in our data from Greenland (Fig. 10).

Microprobe mapping reveals that the schist is now largely berthierine (septechamosite $[(Fe^{2+},Fe^{3+},Al)_3(Si,Al)_2O_5(OH)_4]$). Chemical composition of the schist (Jahren and Aagaard, 1989) also matches berthierine (Fig. 9B). Berthierine is a plausible original soil clay found also in paleosols (Sheldon and Retallack, 2002), but unlikely in view of obvious metamorphic recrystallization (Fig. 4). A common early diagenetic reaction to berthierine from kaolinite and siderite (Ijima and Matsumoto, 1982) is also unlikely considering the high content of magnesium (21 wt% by ion microprobe). A likely precursor clay to berthierine with this much magnesia and ferrous iron (61 wt% determined by ion microprobe) is saponite (iron-magnesium smectite $[Ca_{0.1}Na_{0.1}Mg_{2.25}Fe^{2+}_{0.75}Si_3AlO_{10}(OH)_2{\cdot}4(H_2O)]$). A wide array of chemical compositions of other plausible minerals were compared with our microprobe data, and none is a good match.

Microprobe mapping also reveals that the inclusion-filled, crystal pseudomorphs are the metamorphic mineral ripidolite (ferroan clinochlore $[(Mg,Fe,Al)_6(Si,Al)_4O_{10}(OH)_8]$), These pseudomorphs have insufficient alumina and very different crystal form from cordierite, staurolite, kyanite, sillimanite, or garnet. A plausible origin of these pseudomorphs is as remnants of a soluble salt, like sand crystals common in soils and paleosols (Nabhan et al., 2016; Retallack et al., 2016; Retallack, 2018). That mineral is unlikely to be barite, gypsum or nahcolite, because of the lack of any residual Ca or Ba. Excess Mg in the pseudomorphs (Table 2) can be taken as evidence that the original mineral was kieserite $[MgSO_4{\cdot}H_2O]$, which has a prismatic monoclinic form (Palache et al., 1951), and fits the preserved crystal faces of the sand crystals (Fig. 5). Kieserite can form from highly acidic weathering of basalt (Tosca and McLennan, 2006). Kieserite is stable over a wide range of temperatures and relative humidity, but readily dissolved in water (Chipera and Vaniman, 2007). Partial dissolution and replacement may have been during deposition of the overlying sandstone or early burial of the profile.

7. Reconstructed soil

The putative paleosol is confirmed as not one, but two profiles, with a second profile showing elevated titanium (Fig. 10), and silt-filled, downward tapering, ptygmatically-folded cracks (Fig. 4B–C) in the lowest sample, as seen in the highest sample. This lowest sample is a surface (A) horizon of a paleosol lacking the sand crystals and degree of the chemical or textural development of the upper profile. These two paleosol profiles are here given non-genetic names here using the West Greenlandic language and soil texture of their surface horizons as the Isi clay (upper profile) and Pukit silty clay (lower profile) paleosols. Isi is “eye”, an allusion to field appearance of its lenticular crystal pseudomorphs, and pukit is “short”, in West Greenlandic (Fortescue, 1984).

Table 3
Transfer functions used to interpret Archaean paleosols.

Equation	Variables	Coefficient (R^2)	Standard error	Reference
$\lambda_{j,w} = \left[\frac{\rho_w \cdot C_{j,w}}{\rho_p \cdot C_{j,p}}\right][\varepsilon_{i,w} + 1] - 1$	$\tau_{w,j}$ (mole fraction) = mass transfer of a specified (j) element in a soil horizon (w); ρ_w (g·cm^{-3}) = bulk density of the soil; ρ_p (g·cm^{-3}) = bulk density of parent material; $C_{j,w}$ (weight %) = chemical concentration of an element (j) in a soil horizon (w); $C_{p,w}$ (weight %) = chemical concentration of an element (j) in the parent material (p): $\varepsilon_{i,w}$ (mole fraction) = strain due to soil formation	None	None	Brimhall et al., 1992
$\varepsilon_{i,w} = \left[\frac{\rho_p \cdot C_{i,p}}{\rho_w \cdot C_{i,w}}\right] - 1$	$\varepsilon_{i,w}$ (mole fraction) = strain of a soil horizon (w) with respect to a stable chemical constituent (i); ρ_w (g·cm^{-3}) = bulk density of a soil horizon; ρ_p (g·cm^{-3}) = bulk density of parent material; $C_{i,w}$ (weight %) = chemical concentration of stable element (i) in a soil horizon (w); $C_{p,w}$ (weight %) = chemical concentration of stable element (i) in the parent material (p)	None	None	Brimhall et al., 1992
$CO_2 = \frac{M}{A\left[\frac{K_{CO_2}P}{1000} + \kappa\frac{D_{CO_2}\alpha}{L}\right]}$	pCO_2 (atmospheres) = partial pressure of atmospheric carbon dioxide: M (mol CO_2/cm$_2$) = summed mass transfer losses of MgO, CaO, Na_2O and K_2O through the profile $M = 2\sum \rho_p \frac{C_{j,p}}{100} \int_{Z=0}^{Z=D_{j,w}} \tau_{j,w(z)}\delta Z$; ρ_p (g·cm^{-3}) = bulk density of parent material; $C_{j,p}$ (weight %) = chemical concentration of an element (j) in parent material (p); $\tau_{j,w}$ (mole fraction) = mass transfer of a specified (j) element in a soil horizon (w); Z (cm) = depth in soil represented by analysis; A (years) = duration of soil formation; K_{CO_2} (mol/kg·bar) = Henry's Law constant for CO_2 (=0.034, range 0.031–0.045); P (cm) = mean annual precipitation; κ (s·cm^3/mol·year) = seconds per year divided by volume per mole of gas at standard temperature and pressure (=1409); D_{CO_2} (cm^2/s) = diffusion constant for CO_2 in air (=0.162 at 20 °C, range at 0–40 °C of 0.139–0.181); α (fraction) = ratio of diffusion constant for CO_2 in soil divided by diffusion constant for CO_2 in air (=0.1, range 0.08–0.12); L (cm) = original depth to water table (after decompaction, B below)	None	Tables S6–S7	Sheldon, 2006
$O_2 = \frac{F}{A\left[\frac{K_{O_2}P}{1000} + \kappa\frac{D_{O_2}\alpha}{L}\right]}$	pO_2 = partial pressure of atmospheric oxygen (atmospheres); F (mol CO_2/cm$_2$) = summed mass transfer gains of Fe_2O_3 through the profile $M = 2\sum \rho_p \frac{C_{j,p}}{100} \int_{Z=0}^{Z=D_{j,w}} \tau_{j,w(z)}\delta Z$; ρ_p (g·cm^{-3}) = bulk density of parent material; $C_{j,p}$ (weight %) = chemical concentration of an element (j) in parent material (p); $\tau_{j,w}$ (mole fraction) = mass transfer of a specified (j) element in a soil horizon (w); Z (cm) = depth in soil represented by analysis; A (years) = duration of soil formation; K_{O_2} (mol/kg·bar) = Henry's Law constant for O_2 (=0.00125, range 0.0012–0.0013); P (cm) = mean annual precipitation; κ (s·cm^3/mol·year) = seconds per year divided by volume per mole of gas at standard temperature and pressure (=1409); D_{O_2} (cm^2/s) = diffusion constant for O_2 in air (=0.203 at 20 °C, range from 0 to 40 °C is 0.179–0.227); α (fraction) = ratio of diffusion constant for O_2 in soil divided by diffusion constant for O_2 in air (=0.2, range 0.09–0.32); L (cm) = original depth to water table (after decompaction, B below)	None	Tables S6–S7	Retallack, 2018
$A = 3920 \cdot S^{0.34}$	A (yrs) = duration of soil formation; S = diameter of micritic low-magnesium calcite nodules (cm)	0.57	± 1800 myrs	Retallack, 2005
$A = 3987 \cdot G + 5774$	A (yrs) = duration of soil formation; G = proportion of surface covered by gypsum crystals or nodules (%)	0.95	± 15,000 yrs	Retallack, 2018
$B = \frac{-0.51}{\frac{0.49}{e^{0.27k}} - 1}$	B (fraction) = compaction of Inceptisol due to burial; k (km) = depth of burial	None	None	Sheldon and Retallack, 2001
$P = 221e^{0.0197R}$	P (mm) = mean annual precipitation; R (mol) = 100mAl_2O_3 / (mAl_2O_3 + mCaO + mNa_2O)	0.72	± 182 mm	Sheldon et al., 2002
$T = 0.21I - 8.93$	T (°C) = mean annual paleotemperature; I (mole fraction) = chemical index of weathering $\left(I = \frac{100 \cdot Al_2O_3}{(Al_2O_3 + CaO + Na_2O)}\right)$	0.81	± 0.5 °C	Óskarsson et al., 2012

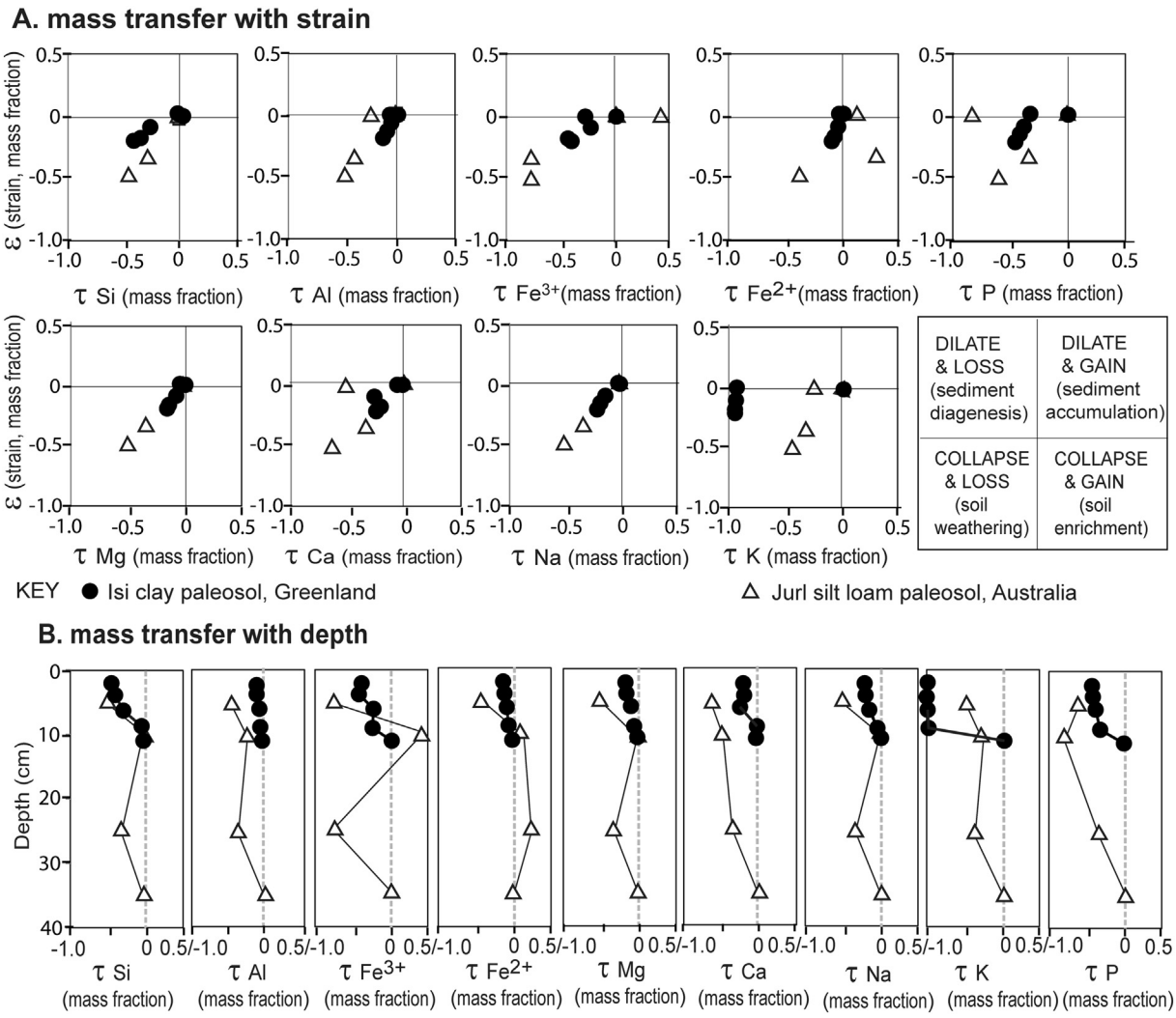

Fig. 10. Geochemical mass balance for 3.7 Ga Isi paleosol from Isukasia, Greenland, compared with Jurl paleosol of Western Australia (Retallack et al., 2016): A, mass fraction deviation from parent material (at origin) in strain and mass transfer; B, deviation of mass transfer from parent material (zero) with depth in paleosol.

8. Paleosol interpretation

Reconstructing protolith composition before metamorphism and as paleosols has been difficult, but it is useful to explore paleoenvironmental implications as paleosols and comparisons with undisputed Archean paleosols. Identification within modern soil classifications gives some basis for interpretation (Table 4), but soil science theory can also be used to reconstruct their 3.7 Ga paleoenvironmental setting and development (Table 5).

8.1. Soil identification

Reconstructed as originally a saponite-kieserite profile, the Isi paleosol would have been a Gypsid in soil taxonomy (Soil Survey Staff, 2014). Gypsids are extreme desert soils with a subsurface By horizon of sulfates (Reheis, 1987; Amundson et al., 2012), but other sulfate soils form in humid climates by acid sulfate weathering (Jennings and Driese, 2014). In the Food and Agriculture Organization (1974) this is a Solonchak soil. The Pukit paleosol on the other hand is a very weakly developed soil, a Fluvent of Soil Survey Staff (2014) or Fluvisol of Food and Agriculture Organization (1974).

A fundamental puzzle of the reconstructed Isi paleosol is large crystals of sulfate, like abundant sulfate crystals and pseudomorphs in many other Archean paleosols (Nabhan et al., 2016; Retallack et al., 2016; Retallack, 2018). How could so much sulfate accumulate under an anoxic atmosphere? Photo-oxidation of sulfite is very slow, but has been modeled for other anoxic planetary atmospheres (Lewis and Kreimendahl, 1980; Tosca and McLennan, 2006). Anaerobic sulfur-

Table 4
Summary of Isukasia paleosol definition and classification.

Pedotype	Greenlandic meaning	Diagnosis	US taxonomy (Soil Survey Staff, 2014)	FAO (1974) map unit
Isi	Eye	Laminated and cracked gray surface (A) horizon over diffuse horizon of large poikiloblastic crystals (By)	Gypsid	Solonchak
Pukit	Short	Laminated and cracked surface (A) horizon over bedded siltstone (C) horizon	Fluvent	Dystric Fluvisol

Note: West Greenlandic definitions are from Fortescue (1984).

Table 5
Summary of Isukasia paleosol interpretation.

Pedotype	Climate and atmospheric composition	Organisms	Topography	Parent material	Soil duration
Isi	Anoxic (36 ± 510 ppm O_2), greenhouse (820 ± 201 ppm CO_2), humid (mean annual precipitation 1561 ± 182 mm), cool temperate (mean annual temperature 11.9 ± 0 .4 °C) paleoclimate	Photosynthetic microbes fractionating organic carbon	Alluvial terrace on floodplain	Alluvial quartzo-feldspathic silt	4876 ± 1800 years
Pukit	Not diagnostic for climate or atmospheric composition	Photosynthetic microbes fractionating organic carbon	Near stream levee of floodplain	Alluvial quartzo-feldspathic silt	< 100 years

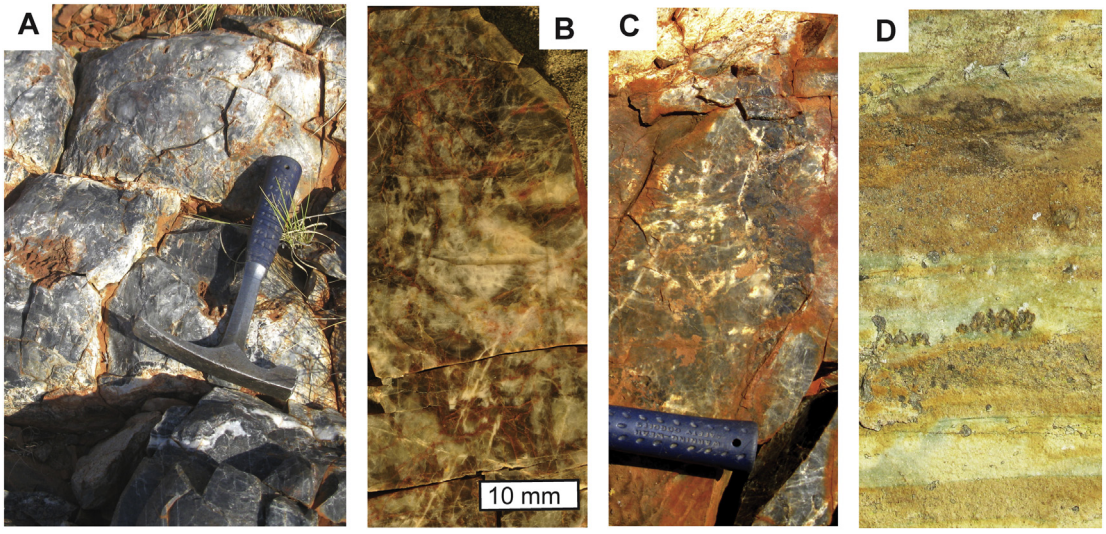

Fig. 11. Comparable paleosols with sand crystals in a subsurface horizon (By) from the Archaean of Western Australia (A–C): including (A), Jurl pedotype with silica pseudomorphs of barite from the 3.0 Ga Farrel Quartzite of Mt. Grant (Retallack et al., 2016), and (B–C) from the 3.5 Ga Panorama Formation of Panorama Portal (Retallack, 2018), and (D) un-named paleosol with gypsum crystals from 3.2 Ga Moodies Group near Barberton, South Africa (Nabhan et al., 2016).

bacterial photosynthesis can produce large amounts of sulfate as a by-product of carbon fixation from CO_2 (Senko et al., 2004; Youssef et al., 2010), but it is premature to infer life in the Isi paleosol. Other Archean paleosols of presumed anoxic atmospheres (Fig. 11) share the following features with the Isi paleosol: drab color, dominantly unoxidized iron and manganese, mafic parent material, sulfate crystals or pseudomorphs, and traces of soil carbon. The Isi paleosol is not unusual in the context of other Archaean paleosols, and so compounds the problem of anoxic sulfate formation.

8.2. Atmospheric composition

The integrated profile gain of iron and manganese can be used to estimate moles of atmospheric O_2 used during soil formation (Retallack, 2018), in a comparable way to using the integrated profile loss of alkali and alkaline earth cations as an indication of atmospheric CO_2 use (Sheldon, 2006). The equations for these calculations (Table 3) may not be appropriate for acid sulfate soils (Retallack, 2018), and involve many variables: observed abundance of carbonic acid-sensitive elements (for pCO_2) and oxygen sensitive elements (for O_2), together with diffusion constants (Denny, 1993; Aachib et al., 2004), depth to water table (corrected for compaction using Sheldon and Retallack, 2001), and estimates of mean annual precipitation and duration of soil formation (also using proxies in Table 3). Soil duration of 4876 years from poikiloblast size (Retallack, 2005), was used rather than 17,735 years from 3% cover of poikiloblasts (Retallack, 2013). Gaussian error propagation for each of the variables is shown in Table S6, and partial derivatives for each component of error calculation in Table S7. These calculations give only 36 ± 510 ppm O_2 and 820 ± 201 ppm CO_2. Sulfur gases also are likely sources of weathering sulfate in solution, and sources of sulfate crystals (Chipera and Vaniman, 2007). These estimates are thus tentative, but not unreasonable from the perspective of what else is known about atmospheric evolution on Earth (Rye and Holland, 1998; Sheldon, 2006).

8.3. Paleoclimate

Soil chemistry of the Isi paleosol can be a guide to paleoprecipitation (Sheldon et al., 2002) and paleotemperature (Óskarsson et al., 2012). Using equations shown in Table 3, the Isi paleosol is chemically similar to soils of modern humid (mean annual precipitation 1561 ± 182 mm) and cool temperate climate (mean annual temperature 12 ± 0.4 °C). The Pukit paleosol is too weakly developed to have a significant chemical signal of paleoclimate.

Acid-sulfate weathering in a humid climate also explains degree of leaching and clayeyness of the profile from molar weathering ratios (Fig. 2). This and ptygmatically folded cracks filled with quartz silt (Fig. 4B, C) are evidence that the top 14 cm of the soil was weathered in a regime of free drainage unimpeded by waterlogging. High ferrous to ferric iron ratios in modern soils (Fig. 3) are now evidence of waterlogging, but in Precambrian paleosols they are found in formerly well drained soils because of low atmospheric oxygen (Retallack et al., 2016, Retallack, 2018).

8.4. Soil parent material

The parent material of the Isi paleosol was a silty claystone very distinct in composition from the enclosing quartzites, and presumably derived from clayey basaltic soils like other Isua metasediments (Fig. 9A). In contrast, the quartzites had a much more felsic source terrane, enriched in large quartz grains in an energetic sedimentary environment such as a braided stream or estuary (Fedo, 2000). The quartzite also includes large clasts of biotite schist (Fig. 4A), presumably from the mountainous southern metamorphic terrane nearby

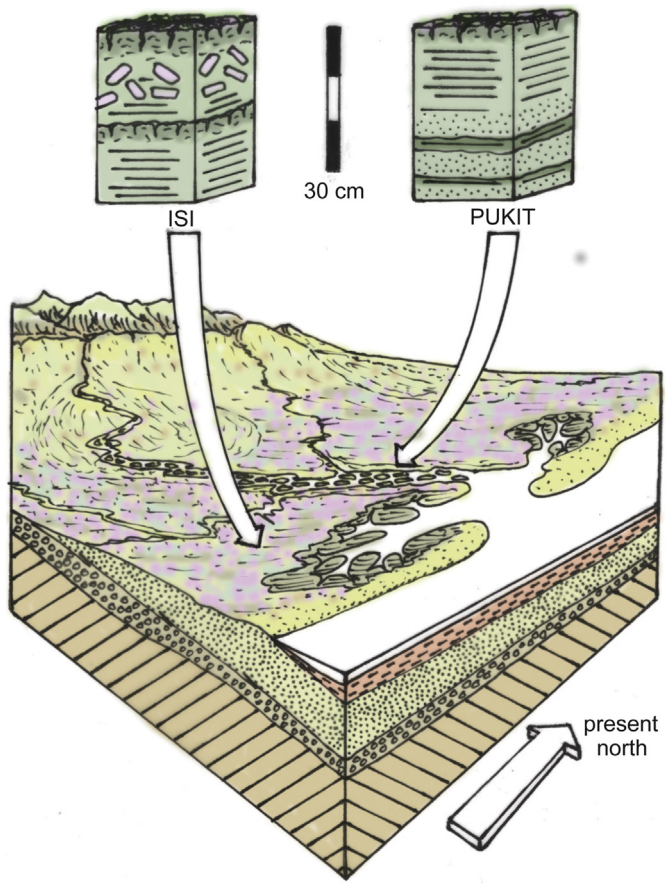

Fig. 12. Reconstructed 3.7 Ga paleosols from Isukasia, West Greenland.

(Fig. 1).

8.5. Paleotopography

The Isi paleosol from Greenland is comparable with other Archean paleosols (Fig. 11) in having evaporitic sand crystals in a subsurface (By) horizon, and other evidence of freely drained weathering, yet little evidence of oxidation during weathering. Many Archean paleosols had gypsum ($CaSO_4{\cdot}2H_2O$) and barite ($BaSO_4$) sand crystals (Nabhan et al., 2016; Retallack et al., 2016; Retallack, 2018). Study of Precambrian paleosols has documented the widespread soil-forming chemical reaction of hydrolysis by carbonic acid from soil carbon dioxide (Rye and Holland, 1998), but other Archean paleosols with sulfate sand crystals open the possibility of an earlier widespread phase of anaerobic acid-sulfate weathering (Amundson et al., 2012; Jennings and Driese, 2014).

Preservation of intact clasts of soft biotite schist (Fig. 4A) is evidence for high relief nearby, probably the southern terrane (Fig. 1). Despite this hilly source terrain, the quartz-rich depositional plain included swales only 40 cm thick filled with clay (Fig. 12). The ubiquitous quartzite with trough cross bedding and shallow lens of claystone is a facies comparable with that of sandy braided streams (Conaghan, 1980).

8.6. Time for formation

Modest clay enrichment and salt crystals averaging 1.9 ± 0.4 cm long would have taken thousands of years to form in soil. Similar modern Aridisol calcite nodule sizes are reached after only 4876 ± 1800 years (Retallack, 2005). Accumulation of pedogenic gypsum to such size and density in soils also takes millennia (Amundson et al., 2012; Retallack, 2013; Jennings and Driese, 2014). There is no known chronofunction for kieserite in modern soils.

8.7. Life on land?

The principal line of evidence for life during deposition of the Isua supercrustal sequence has been isotopically light carbon within the range −29.6‰ to −6.5‰, thought to have been depleted largely by photosynthesis, and only slightly enriched by metamorphism (Rosing, 1999; Grassineau et al., 2006). Evidence that some of this organic carbon was from Holocene endolithic organisms (Westall and Folk, 2003) or secondary carbonate veins (van Zuilen et al., 2003), has now been dispelled by TEM studies (Ohtomo et al., 2014) and discovery of graphitized organic matter within relict trails of ca. 3.7 Ga metamorphic garnets of the Isua region (Hassenkam et al., 2017). Our outcrops were unusually clean of secondary veins (Fig. 2A), lichens or other contaminating organisms (Fig. 2A), and our thin sections showed no trace of endolithic organisms (Fig. 4).

Our analytical results for organic carbon within the Isi paleosol show only trace amounts of organic carbon (0.02 to 0.09%) and $\delta^{13}C$ of −24.2 to −27.4‰ (Fig. 3C). This is much less varied than other Greenland carbon isotopic values in sedimentary rocks (Grassineau et al., 2006), and furthermore shows a muted upward lightening trend like other analyses of paleosols (Retallack, 2007). The two paleosol surfaces are heavy compared with below, and there is a muted upward-lightening (negative) trend between the two. The Rayleigh distillation process of mass-dependent decay of organic matter produces isotopically heavy carbon deep in soils from isotopically light carbon of photosynthesis near the surface (Wynn, 2007). From this perspective each paleosol surface has a litter of decayed organic matter, and below that freshly photosynthesized carbon increasingly decayed down the profile. If the organic matter analyzed by us were modern contamination, the muted variation parallel with other weathering indices are a surprising coincidence. Our data is not conclusive evidence of life in the paleosol, but suggestive, and additional ultrastructural studies like those of Hassenkam et al. (2017) are warranted.

Past carbon isotopic studies of Isua graphites have assumed that life at 3.7 Ga was entirely marine (Grassineau et al., 2006; Ohtomo et al., 2014), but systematic muted variation within our thin profile is compatible with life on land. The consistency of these data are also evidence against organic carbon compounds in the schist forming abiotically, as in meteorites with adjacent kerogen grains of very different isotopic compositions (Amari et al., 1993). Furthermore, our data are from a paleosol with geochemical evidence (Figs. 2–4) of formation on dry land, and not an ancient aquatic community of hydrothermal vents (Dodd et al., 2017) or terrestrial springs (Djokic et al., 2017). Hydrothermal graphite and microstructures from northern Quebec dated to 3.8–4.3 Ga (Dodd et al., 2017) may be earlier evidence of marine aquatic life on Earth than our paleosol. The distinction whether the earliest life was in the sea, in marine black smokers, in freshwater springs, in lakes and ponds, or in well-drained soils is relevant to theories of the origin of life (Retallack, 2016a).

9. Conclusions

The paleosol hypothesis for the schist bed was not ruled out by our eight tests: field appearance, crack fills, textural profile, mineral profile, molar ratios, carbon isotopic composition, REE trends, and tau analysis. Considered as paleosols, they have been classified and given non-genetic field names from the West Greenlandic language, and reconstructed for the various soil-forming factors evident from their morphology, petrographic and geochemical composition. With a geological age of 3.7 Ga, these putative paleosols may be the oldest known evidence for soil-forming processes. The topographic setting of the paleosols is envisaged as a narrow coastal plain of braided streams between a stromatolitic continental shelf and mountains. The paleosols accumulated sulfate sand crystals, of a size found in modern well-

drained soils over periods of several thousand years (4876 ± 1800 years). Chemical composition of the profile is like that of modern humid (mean annual precipitation 1561 ± 182 mm) and cool temperate (mean annual temperature 12 ± 0.4 °C) soils. The distribution of acid-soluble elements in the profile are evidence of high levels (820 ± 201 ppm) of atmospheric CO_2, and the distribution of oxides within the profile reveal low levels (36 ± 510 ppm) of atmospheric O_2. Muted variation of organic $\delta^{13}C$ (−24.2 to −27.4‰) in a depth function comparable with other weathering functions is suggestive evidence of life in the soil, and additional ultrastructural tests of this organic matter are warranted.

Acknowledgments

Fieldwork by NN was funded by NSF EAR 0929617. Laboratory work including bulk density determination by GJR was funded by University of Oregon Academic Support Award. Chemical analyses were by ALS Global of Vancouver, British Columbia. Electron microprobe work was done by J. Donovan, Center for Advanced Materials Characterization at Oregon (CAMCOR) of the University of Oregon, and carbon isotopic analyses by M. Yun of the University of Manitoba We are grateful for discussions with Bruce Runnegar, Steven Driese, Kathleen Benison, Martin Van Kranendonk, Malcolm Walter, James Farquhar, and Roger Buick.

Appendix A. Supplementary data

Supplementary data to this article can be found online at https://doi.org/10.1016/j.palaeo.2018.10.005.

References

Aachib, M., Mbonimpa, M., Aubertin, M., 2004. Measurement and prediction of the oxygen diffusion coefficient in unsaturated media with applications to soil covers. Water Air Soil Pollut. 156, 163–193.
Amari, S., Hoppe, P., Zinner, E., Lewis, R.S., 1993. The isotopic compositions and stellar sources of meteoritic graphite grains. Nature 365, 806.
Amundson, R., Dietrich, W., Bellugi, D., Ewing, S., Nishiizumi, K., Chong, G., Owen, J., Finkel, R., Heimsath, A., Stewart, B., Caffee, M., 2012. Geomorphological evidence for the late Pliocene onset of hyperaridity in the Atacama Desert. Geol. Soc. Am. Bull. 124, 1048–1070.
Appel, P.W.U., 1983. Rare earth elements in the Early Archean Isua Iron Formation, West Greenland. Precambrian Res. 20, 243–258.
Arai, T., Omori, S., Komiya, T., Maruyama, S., 2015. Intermediate P/T-type regional metamorphism of the Isua Supracrustal Belt, southern west Greenland: the oldest Pacific-type orogenic belt? Tectonophysics 662, 22–39.
Armstrong, J.T., 1988. Quantitative analyses of silicates and oxide minerals: comparison of Monte-Carlo, ZAF and Phi-Rho-Z procedures. In: Rothwell, T.E., Russell, P.E. (Eds.), Microbeam Analysis. San Francisco Press, San Francisco, pp. 239–246.
Benison, K.C., Bowen, B.B., 2013. Extreme sulfur-cycling in acid brine lake environments of Western Australia. Chem. Geol. 351, 154–167.
Benison, K.C., Bowen, B.B., 2015. The evolution of end-member continental waters: the origin of acidity in southern Western Australia. GSA Today 25, 4–10.
Bolhar, R., Kamber, B.S., Moorbath, S., Whitehouse, M.J., Collerson, K.D., 2005. Chemical characterization of earth's most ancient clastic metasediments from the Isua Greenstone Belt, southern West Greenland. Geochim. Cosmochim. Acta 69, 1555–1573.
Brewer, R., 1974. Fabric and Mineral Analysis of Soils. Krieger, New York (482 pp.).
Brimhall, G.H., Chadwick, O.A., Lewis, C.J., Compston, W., Williams, I.S., Danti, K.J., Dietrich, W.E., Power, M.E., Hendricks, D., Bratt, J., 1992. Deformational mass transport and invasive processes in soil evolution. Science 255, 695–702.
Buick, R., Dunlop, J.S.R., 1990. Evaporitic sediments of early Archean age from the Warrawoona Group, North Pole, Western Australia. Sedimentology 37, 247–277.
Certini, G., Ugolini, F.C., 2013. An updated, expanded, universal definition of soil. Geoderma 192, 378–379.
Chipera, S.J., Vaniman, D.T., 2007. Experimental stability of magnesium sulfate hydrates that may be present on Mars. Geochim. Cosmochim. Acta 71, 241–250.
Conaghan, P.J., 1980. The Hawkesbury Sandstone: gross characteristics and depositional environment. In: Herbert, C., Helby, R.J. (Eds.), A Guide to the Sydney Basin. Geol. Surv. New South Wales Bull. 26pp. 188–253.
Crowe, S.A., Jones, C., Katsev, S., Magen, C., O'Neill, A.H., Sturm, A., Canfield, D.E., Haffner, G.D., Mucci, A., Sundby, B., Fowle, D.A., 2008. Photoferrotrophs thrive in an Archean Ocean analogue. Proc. Natl. Acad. Sci. 105, 15938–15943.
Denny, M.W., 1993. Air and Water: The Biology and Physics of Life's Media. Princeton Univ. Press, Princeton (366 pp.).
Djokic, T., Van Kranendonk, M.J., Campbell, K.A., Walter, M.R., Ward, C.R., 2017. Earliest signs of life on land preserved in ca. 3.5 Ga hot spring deposits. Nat. Commun. 8, 15263. https://doi.org/10.1038/ncomms15263.
Dodd, M.S., Papineau, D., Grenne, T., Slack, J.F., Rittner, M., Pirajno, F., O'Neil, J., Little, C.T., 2017. Evidence for early life in Earth's oldest hydrothermal vent precipitates. Nature 543, 60.
Donovan, J.J., Tingle, T.N., 1996. An improved mean atomic number correction for quantitative microanalysis. J. Microsc. 2, 1–7.
Donovan, J.J., Snyder, D.A., Tivers, M.L., 1993. An improved interference correction for trace element analysis. Microbeam Anal. 2, 23–28.
Donovan, J.J., Singer, J.W., Armstrong, J.T., 2016. A new EPMA method for fast trace element analysis in simple matrices. Am. Mineral. 101, 1839–1853.
Evans, D.J., White, S.H., 1984. Microstructural and fabric studies from the rocks of the Moine Nappe, Eriboll, NW Scotland. J. Struct. Geol. 6, 369–389.
Fedo, C.M., 2000. Setting and origin for problematic rocks from the > 3.7 Ga Isua Greenstone Belt, southern West Greenland: earth's oldest coarse siliciclastic sediments. Precambrian Res. 101, 69–78.
Food and Agriculture Organization, 1974. Soil Map of the World. Volume I: Legend. U.N.E.S.C.O., Paris (59 pp.).
Fortescue, M., 1984. West Greenlandic. Croom Helm, London (377 pp.).
Goscombe, B.D., Passchier, C.W., 2003. Asymmetric boudins as shear sense indicators—an assessment from field data. J. Struct. Geol. 25, 575–589.
Grassineau, N.V., Abell, P., Appel, P.W.U., Lowry, D., Nisbet, E.G., 2006. Early life signatures in sulfur and carbon isotopes from Isua, Barberton, Wabigoon (Steep Rock), and Belingwe Greenstone Belts (3.8 to 2.7 Ga). In: Kesler, S.E., Ohmoto, H. (Eds.), Evolution of Early Earth's Atmosphere, Hydrosphere, and Biosphere—Constraints from Ore Deposits. Geol. Soc. America Mem., vol. 198. pp. 33–52.
Hannington, M.D., Kjarsgaard, I.M., Galley, A.G., Taylor, B., 2003. Mineral-chemical studies of metamorphosed hydrothermal alteration in the Kristineberg volcanogenic massive sulfide district, Sweden. Mineral. Deposita 38, 423–442.
Hassenkam, T., Andersson, M.P., Dalby, K.N., Mackenzie, D.M.A., Rosing, M.T., 2017. Elements of Eoarchean life trapped in mineral inclusions. Nature 548, 78–81.
Ijima, A., Matsumoto, R., 1982. Berthierine and chamosite in coal measures of Japan. Clay Clay Miner. 30, 264–274.
Jahren, J.S., Aagaard, P., 1989. Compositional variations in diagenetic chlorites and illites, and relationships with formation-water chemistry. Clay Miner. 24, 157–170.
Jennings, D.S., Driese, S.G., 2014. Understanding barite and gypsum precipitation in upland acid-sulfate soils: an example from a Lufkin Series toposequence, south-central Texas, U.S.A. Sediment. Geol. 299, 106–118.
Konhauser, K.O., Hamade, T., Raiswell, R., Morris, R.C., Ferris, F.G., Southam, G., Canfield, D.E., 2002. Could bacteria have formed the Precambrian banded iron formations? Geology 30, 1079–1082.
Lewis, J.S., Kreimendahl, F.A., 1980. Oxidation state of the atmosphere and crust of Venus from Pioneer Venus results. Icarus 42, 330–337.
Loucks, R.R., Lemish, J., Damon, P.E., 1988. Polymetallic epithermal fissure vein mineralization, Topia, Durango, Mexico; part I, district geology, geochronology, hydrothermal alteration, and vein mineralogy. Econ. Geol. 83, 1499–1527.
Lowe, D.R., Worrell, G.F., 1999. Sedimentology, mineralogy, and implications of silicified evaporites in the Kromberg Formation, Barberton Greenstone Belt, South Africa. In: Lowe, D.R., Byerly, G.R. (Eds.), Geologic Evolution of the Barberton Greenstone Belt, South Africa. Geol. Soc. Amer. Spec. Publ., vol. 329. pp. 167–188.
Murphy, C.P., 1983. Point counting pores and illuvial clay in thin section. Geoderma 31, 133–150.
Nabhan, S., Luber, T., Scheffler, T., Heubeck, C., 2016. Climatic and geochemical implications of Archean pedogenic gypsum in the Moodies Group (~3.2 Ga), Barberton Greenstone Belt, South Africa. Precambrian Res. 275, 119–134.
Novoselov, A.A., de Souza Filho, C.R., 2015. Potassium metasomatism of Precambrian paleosols. Precambrian Res. 262, 67–83.
Nutman, A.P., Friend, C.R.L., 2009. New 1:20,000 scale geological maps and history of investigation of the Isua supracrustal belt and adjacent orthogneisses, southern West Greenland: a glimpse of Eoarchaean crust formation and orogeny. Precambrian Res. 172, 189–211.
Nutman, A.P., Bennett, V.C., Friend, C.R.L., 2012. Waves and weathering at 3.7 Ga: geological evidence for an equitable terrestrial climate under the faint early sun. Aust. J. Earth Sci. 89, 167–176.
Nutman, A.P., Bennett, V.C., Friend, C.R.L., 2015. The emergence of the Eoarchaean proto-arc: evolution of a c. 3700 Ma convergent plate boundary at Isua, southern West Greenland. In: Roberts, N.M.W., Van Kranendonk, M., Parman, S., Shirey, S., Clift, P.D. (Eds.), Continent Formation Through Time. Geol. Soc. London Spec. Publ., vol. 389. pp. 113–133.
Nutman, A.P., Bennett, V.C., Friend, C.R., Van Kranendonk, M.J., Chivas, A.R., 2016. Rapid emergence of life shown by discovery of 3,700-million-year-old microbial structures. Nature 537, 535–538.
Ohtomo, Y., Kakegawa, T., Ishida, A., Nagase, T., Rosing, M.T., 2014. Evidence for biogenic graphite in early Archean Isua metasedimentary rocks. Nat. Geosci. 7, 25–28.
Óskarsson, B.V., Riishuus, M.S., Arnalds, O., 2012. Climate-dependent chemical weathering of volcanic soils in Iceland. Geoderma 189–190, 635–651.
Palache, C., Berman, H., Frondel, C., 1951. The System of Mineralogy: Vol II. Halides, Nitrates, Borates, Carbonates, Sulfates, Phosphates, Arsenates, Tungstates, Molybdates, Etc. Wiley, New York (1124 pp.).
Pufahl, P.K., Pirajno, F., Hiatt, E.E., 2013. Riverine mixing and fluvial iron formation: a new type of Precambrian biochemical sediment. Geology 41, 1235–1238.
Reed, J.J., 1964. Mylonites, cataclasites, and associated rocks along the Alpine Fault, South Island, New Zealand. N. Z. J. Geol. Geophys. 7, 645–684.
Reheis, M.C., 1987. Gypsic soils in Kane alluvial fans, Big Horn County, Wyoming. U.S. Geol. Surv. Bull. 1590C, 39.
Retallack, G.J., 2005. Pedogenic carbonate proxies for amount and seasonality of

precipitation in paleosols. Geology 33, 333–336.
Retallack, G.J., 2007. Paleosols. In: Henke, W., Tattersall, I., Hardt, T. (Eds.), Handbook of Paleoanthropology. Springer, Berlin, pp. 383–408.
Retallack, G.J., 2010. Lateritization and bauxitization events. Econ. Geol. 105, 655–667.
Retallack, G.J., 2013. Ediacaran life on land. Nature 493, 89–92.
Retallack, G.J., 2016a. Astropedology: paleosols and the origin of life. Geol. Today 32, 172–178.
Retallack, G.J., 2016b. Field and laboratory tests for recognition of Ediacaran paleosols. Gondwana Res. 36, 94–110.
Retallack, G.J., 2018. Oldest recognized paleosols on Earth, Panorama Formation (3.46 Ga), Western Australia. Palaeogeogr. Palaeoclimatol. Palaeoecol. 489, 230–248.
Retallack, G.J., Bestland, E.A., Fremd, T.J., 2000. Eocene and Oligocene paleosols and environmental change in central Oregon. In: Geol. Soc. Amer. Spec. Pap. 344, (192 pp.).
Retallack, G.J., Krinsley, D.H., Fischer, R., Razink, J.J., Langworthy, K., 2016. Archean coastal-plain paleosols and life on land. Gondwana Res. 40, 1–20.
Rollinson, H., 2002. The metamorphic history of the Isua Greenstone Belt, Greenland. In: Fowler, C.M.R., Ebinger, C.J., Hawkesworth, C.J. (Eds.), The Early Earth: Physical, Chemical and Biological Development. Geol. Soc. London Spec. Publ., vol. 199. pp. 329–350.
Rosing, M.T., 1999. ^{13}C-depleted carbon microparticles in > 3700-Ma sea-floor sedimentary rocks from West Greenland. Science 283, 674–678.
Rye, R., Holland, H.D., 1998. Paleosols and the evolution of atmospheric oxygen: a critical review. Am. J. Sci. 298, 621–672.
Schenk, O., Urai, J.L., van der Zee, W., 2007. Evolution of boudins under progressively decreasing pore pressure–a case study of pegmatites enclosed in marble deforming at high grade metamorphic conditions, Naxos, Greece. Am. J. Sci. 307, 1009–1033.
Senko, J.M., Campbell, B.S., Henriksen, J.R., Elshahed, M.S., Dewers, T.A., Krumholz, L.R., 2004. Barite deposition resulting from phototrophic sulphide-oxidizing bacterial activity. Geochim. Cosmochim. Acta 68, 773–780.
Sheldon, N.D., 2006. Precambrian paleosols and atmospheric CO_2 levels. Precambrian Res. 147, 148–155.
Sheldon, N.D., Retallack, G.J., 2001. Equation for compaction of paleosols due to burial. Geology 29, 247–250.
Sheldon, N.D., Retallack, G.J., 2002. Low oxygen levels in earliest Triassic soils. Geology 30, 919–922.
Sheldon, N.D., Retallack, G.J., Tanaka, S., 2002. Geochemical climofunctions from North American soils and application to paleosols across the Eocene-Oligocene boundary in Oregon. J. Geol. 110, 687–696.
Soil Survey Staff, 2014. Keys to Soil Taxonomy. Natural Resources Conservation Service, Washington (600 pp.).
Sugahara, H., Sugitani, K., Mimura, K., Yamashita, F., Yamamoto, K., 2010. A systematic rare-earth elements and yttrium study of Archean cherts at the Mount Goldsworthy greenstone belt in the Pilbara Craton: implications for the origin of microfossil-bearing black cherts. Precambrian Res. 177, 73–87.
Tosca, N.J., McLennan, S.M., 2006. Chemical divides and evaporite assemblages on Mars. Earth Planet. Sci. Lett. 241, 21–31.
van Zuilen, M.A., Lepland, A., Teranes, J., Finarelli, J., Wahlen, M., Arrhenius, G., 2003. Graphite and carbonates in the 3.8 Ga old Isua Supracrustal Belt, southern West Greenland. Precambrian Res. 126, 331–348.
Westall, F., Folk, R.L., 2003. Exogenous carbonaceous microstructures in Early Archaean cherts and BIFs from the Isua Greenstone Belt: implications for the search for life in ancient rocks. Precambrian Res. 126, 313–330.
Wynn, J.G., 2007. Carbon isotope fractionation during decomposition of organic matter in soils and paleosols: implications for paleoecological interpretations of paleosols. Palaeogeogr. Palaeoclimatol. Palaeoecol. 251, 237–248.
Youssef, N.H., Couger, M.B., Elshahed, M.S., 2010. Fine-Scale bacterial beta diversity within a complex ecosystem (Zodletone Spring, OK, USA): the role of the rare biosphere. PLoS One 5, e12414.